

Alternating-spin $S = \frac{3}{2}$ and $\sigma = \frac{1}{2}$ Heisenberg chain with three-body exchange interactions

N. B. Ivanov^{1,2}, S. I. Petrova³, and J. Schnack¹

¹ Department of Physics, Bielefeld University, P.O. box 100131, D-33501 Bielefeld, Germany

² Institute of Solid State Physics, Bulgarian Academy of Sciences, Tzarigradsko chaussee 72, 1784 Sofia, Bulgaria

³ Department of Engineering Sciences and Mathematics, University of Applied Sciences, D-33619 Bielefeld, Germany

Received: date / Revised version: date

Abstract. The promotion of collinear classical spin configurations as well as the enhanced tendency towards nearest-neighbor clustering of the quantum spins are typical features of the frustrating isotropic three-body exchange interactions in Heisenberg spin systems. Based on numerical density-matrix renormalization group calculations, we demonstrate that these extra interactions in the Heisenberg chain constructed from alternating $S = 3/2$ and $\sigma = \frac{1}{2}$ site spins can generate numerous specific quantum spin states, including some partially-polarized ferrimagnetic states as well as a doubly-degenerate non-magnetic gapped phase. In the non-magnetic region of the phase diagram, the model describes a crossover between the spin-1 and spin-2 Haldane-type states.

PACS. 75.10.Jm Quantized spin models – 75.40.Mg Numerical simulation studies – 75.45.+j Macroscopic quantum phenomena in magnetic systems

1 Introduction

The biquadratic spin-spin interactions $(\mathbf{S}_i \cdot \mathbf{S}_j)^2$ and the three-spin exchange couplings $(\mathbf{S}_i \cdot \mathbf{S}_j)(\mathbf{S}_i \cdot \mathbf{S}_k) + h.c.$ ($|\mathbf{S}_i| > \frac{1}{2}$, $i \neq j, k$; $j \neq k$) naturally appear in the fourth order of the strong-coupling expansion of the two-orbital Hubbard model [1]. Since in this case both types of couplings are controlled by one and the same model parameter – which is about two orders of magnitude weaker than the principal Heisenberg coupling – it might be a challenge to identify experimentally accessible systems where the effects of higher-order interactions can be definitely isolated. Unlike the biquadratic exchange couplings [2], so far there is no clear evidence for effects in real systems related to three-body exchange interactions, although possible three-body exchange effects in some magnetic molecules [3,4] and in the spin- $\frac{5}{2}$ Heisenberg chain $\text{CsMn}_x\text{Mg}_{1-x}\text{Br}_3$ [5] have been discussed.

On the theoretical side, only recently some specific features of the three-body exchange interaction in Heisenberg spin models in space dimensions $D=1$ [1,6,7,8] and $D=2$ [9,13,14] have been discussed in the literature. In particular, two of us (N.B.I and J.S) recently analyzed the full quantum phase diagram of the alternating-spin Heisen-

berg chain [7] defined by the Hamiltonian

$$\mathcal{H} = J_1 \sum_{n=1}^L \mathbf{S}_{2n} \cdot (\boldsymbol{\sigma}_{2n-1} + \boldsymbol{\sigma}_{2n+1}) + J_2 \sum_{n=1}^L [(\mathbf{S}_{2n} \cdot \boldsymbol{\sigma}_{2n-1})(\mathbf{S}_{2n} \cdot \boldsymbol{\sigma}_{2n+1}) + h.c.], \quad (1)$$

in the extremely quantum case of on-site spins $S = 1$ and $\sigma = \frac{1}{2}$. Here $J_1 = \cos \theta$, $J_2 = \sin \theta$ ($0 \leq \theta < 2\pi$), and L denotes the number of unit cells containing two different spins ($S > \sigma$). The model provides a simple, but realistic, example of a Heisenberg system with three-body exchange interactions. For the class of models with $\sigma = \frac{1}{2}$ the biquadratic terms $(\boldsymbol{\sigma}_i \cdot \mathbf{S}_j)^2$ reduce to bilinear Heisenberg spin-spin interactions, so that Eq. (1) represents already the general form of the alternating-spin Heisenberg chain with higher-order isotropic exchange interactions.

In this article, we analyze the quantum phase diagram of the above model for the pair of local spins $S = \frac{3}{2}$ and $\sigma = \frac{1}{2}$. Our motivation for this work follows from a previously established tendency towards formation of composite spins from the local S and σ spins in the unit cell—an effect of the three-body exchange interactions in the region $\frac{\pi}{4} < \theta < \frac{3\pi}{4}$ of the classical phase diagram, which is characterized by a macroscopic (2^L) degeneracy of the ground state (GS) [7]. Therefore, one may expect completely different phase diagrams for systems with integer

and half-integer total spin ($S + \sigma$) in the unit cell, especially in the highly degenerate classical region. Based on density-matrix renormalization group (DMRG) simulations, in the next Section we analyze the quantum phase diagram of the model (1) with $S = \frac{3}{2}$ and $\sigma = \frac{1}{2}$ and discuss different properties of the phases appearing in the interval $0 < \theta < \pi$. The last Section contains a summary of the results.

2 Quantum phase diagram

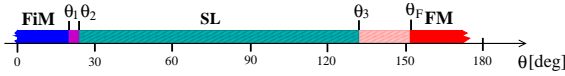


Fig. 1. (Color online) Quantum phase diagram of the model (1) for $S = \frac{3}{2}$ and $\sigma = \frac{1}{2}$ in the interval $0 < \theta < \pi$: The regions $\theta < \theta_1$ and $\theta > \theta_F$ are occupied, respectively, by the Néel ferrimagnetic (FiM) and ferromagnetic (FM) phases, whereas the intervals $\theta_1 < \theta < \theta_2$ and $\theta_3 < \theta < \theta_F$ are occupied by different types of partially-polarized magnetic states. A large parameter region, $\theta_2 < \theta < \theta_3$, is occupied by a non-magnetic doubly-degenerate gapped phase (SL). The FM point $\theta_F = \pi - \arctan(\frac{1}{2}) \approx 153.43^\circ$ is an exact boundary of the FM state, $\theta_1 = 20.1^\circ$, $\theta_2 = 25.5^\circ$, and $\theta_3 \approx 132^\circ$.

The general structure of the phase diagram, as well as the accepted abbreviations for the phases, are presented in Figure 1. Most of the results in this section are obtained through DMRG simulations by performing seven sweeps and keeping up to 500 states in the last sweep [10,11,12]. This ensures a good convergence with a discarded weight of the order of 10^{-8} or better. The numerical DMRG analysis of the lowest energy eigenvalues $E(M)$ in sectors with a fixed z component of the total spin M imply (i) a doubly-degenerate non-magnetic gapped GS (SL) in the interval $\theta_2 < \theta < \theta_3$ and (ii) a number of specific partially-polarized magnetic states in the intervals $\theta_1 < \theta < \theta_2$ and $\theta_3 < \theta < \theta_F$. Many features of the phase diagram in Figure 1 are also encoded in the behavior of the short-range correlations (SRC) for open boundary conditions (OBC) (see Figure 2). In particular, most of the phase boundary points in Figure 1 can be associated with pronounced rearrangements of the SRC. As in the previously studied extreme quantum case of Eq. (1) with $S = 1$ and $\sigma = \frac{1}{2}$ [7], the basic rearrangements concern the SRC between the larger S spins, whereas – apart from the region close to the FM point θ_F – the SRC between the $\sigma = \frac{1}{2}$ spins remain almost constant.¹ The tendency towards spin clustering is revealed by different values of the spin-spin correlators $C_L = \langle \sigma_{2n-1} \cdot \mathbf{S}_{2n} \rangle$ and $C_R = \langle \mathbf{S}_{2n} \cdot \sigma_{2n+1} \rangle$ in the SL state (see Figure 2).

¹ The equation for the exact FM boundary θ_F for arbitrary spins S and σ reads $\cos \theta_F + \sigma (2S + 1) \sin \theta_F = 0$ [7].

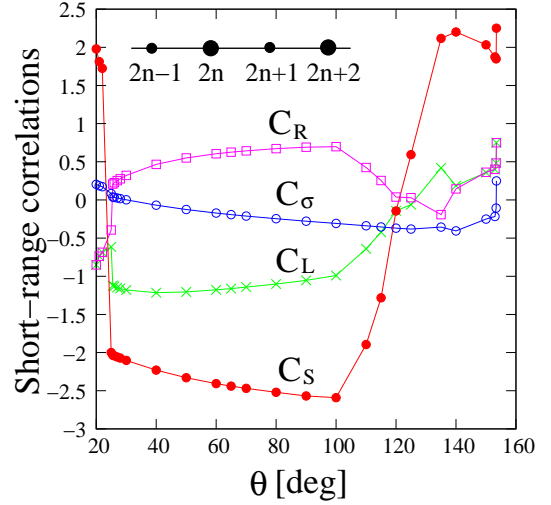


Fig. 2. (Color online) Short-range spin-spin correlations of the ($\frac{3}{2}, \frac{1}{2}$) chain *vs* θ (DMRG, OBC, $L=24$). $C_L \equiv \langle \sigma_{2n-1} \cdot \mathbf{S}_{2n} \rangle$, $C_R \equiv \langle \mathbf{S}_{2n} \cdot \sigma_{2n+1} \rangle$, $C_\sigma \equiv \langle \sigma_{2n-1} \cdot \sigma_{2n+1} \rangle$, and $C_S \equiv \langle \mathbf{S}_{2n} \cdot \mathbf{S}_{2n+2} \rangle$; $n = 1, \dots, L$.

2.1 Partially-polarized magnetic states

The established partially-polarized magnetic states in the intervals $\theta_1 < \theta < \theta_2$ and $\theta_3 < \theta < \theta_F$ do not appear in the classical phase diagram. The critical FiM phase in the first interval is identical to the partially-polarized phase discussed for the extreme quantum case (S, σ) = (1, $\frac{1}{2}$) [7]: It is characterized by a monotonically decreasing magnetization from $m_0 = (S - \sigma) = 1$ at $\theta = \theta_1$ down to $m_0 = 0$ at the phase boundary θ_2 with the non-magnetic phase. At the phase boundary θ_1 the gap of the AFM branch of excitations $\Delta_A = E(M_0 + 1) - E(M_0)$ vanishes and the system becomes critical. Here $M_0 = (S - \sigma)L$ corresponds to the GS of the Lieb-Mattis FiM. Unlike the extreme quantum case, where the phase boundary θ_2 marks the transition to a gapless critical phase, here θ_2 is related with the vanishing of the triplet gap Δ_T of the non-magnetic phase SL. Skipping further discussions on this interesting FiM critical state, we only mention that similar partially-polarized (non-Lieb-Mattis-type) FiM phases have been identified and studied in other spin models, as well [15,16,17].

Now, let us turn to the magnetic states stabilized in the interval $\theta_3 < \theta < \theta_F$ close to the FM point θ_F . The exact phase boundary θ_F coincides with one of the instability points of the one-magnon FM excitations and is characterized by a complete softening of the dispersion function in the whole Brillouin zone. As a result, one observes a strong reconstruction of the FM state for smaller values of θ . As a matter of fact, for $\theta < \theta_F$ we observe a behavior of the SRC which is similar to one in the extreme quantum system (see Figure 4b in Ref. [7]). For this reason, we shall restrict our discussion mainly to the region which is extremely close to the FM point θ_F , as it is natural to expect that the formation of specific plateau states depends on the values of the local spins: According to the general rule, the number of unit cells in the periodic structure q

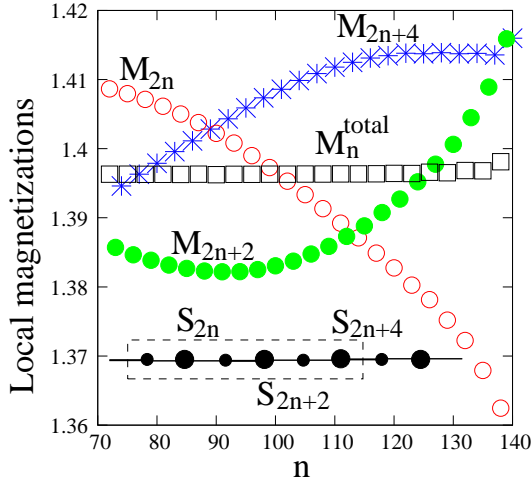


Fig. 3. (Color online) On-site magnetizations $M_k = \langle S_k^z \rangle$ ($k = 2n, 2n+2, 2n+4$) and $M_n^{\text{total}} \equiv (M_{2n} + M_{2n+2} + M_{2n+4})/3$ as functions of the cell index n (DMRG, $\theta = 153.4^\circ$, $L = 144$, OBC). The results indicate a periodic three-cell ($q = 3$) magnetic structure close to the FM transition point θ_F . The Inset shows the magnetic supercell containing six spins (i.e., three unit cells). The total magnetization M_n^{total} in the supercell is constant.

and the magnetic moment per unit cell m_0 of the plateau states fulfill the equation $q(S + \sigma - m_0) = \text{integer}$ [18].

In Figure 3 we show DMRG results for some local magnetic moments related to the S spins at $\theta = 153.4^\circ$, i.e., extremely close to the exact FM boundary θ_F . The results clearly indicate a periodic magnetic structure with a period of three unit cells. As required for a plateau state, the established magnetization at this point, $m_0 = \frac{5}{3}$, fulfills the mentioned general rule with $q = 3$. The DMRG results for Δ_A at $\theta = 153.4^\circ$ shown in Figure 4 give further support for the suggested plateau state since the gap is very small but definitely non-zero. Unfortunately, due to strong finite-size effects, it is difficult to decide if the indicated state is realized only at $\theta = \theta_F$, or in a small interval close to this point. Further, as in the extreme quantum case, the nearest-neighbor spin-spin correlator C_S remains positive and signals a FM ordering of the spin- S subsystem in the entire interval $\theta_3 < \theta < \theta_F$. The transition to a non-magnetic state is accompanied by an abrupt change of the sign of the correlator C_S . Approaching the transition point θ_3 , the boundary effects in open chains become stronger, so that by using DMRG simulations it is difficult to study the vicinity of θ_3 and to fix more precisely its position.

2.2 The non-magnetic SL phase

The numerical results presented in Figure 2 show that for OBC the non-magnetic phase (SL) occupying the interval $\theta_2 < \theta < \theta_3$ is characterized by different nearest-neighbor spin-spin correlations, $C_L \neq C_R$. Excluding some vicinity of the phase boundary θ_3 , the numerical estimates for C_L are located near the eigenvalue $-\frac{5}{4}$ of the operator σ_{2n-1} .

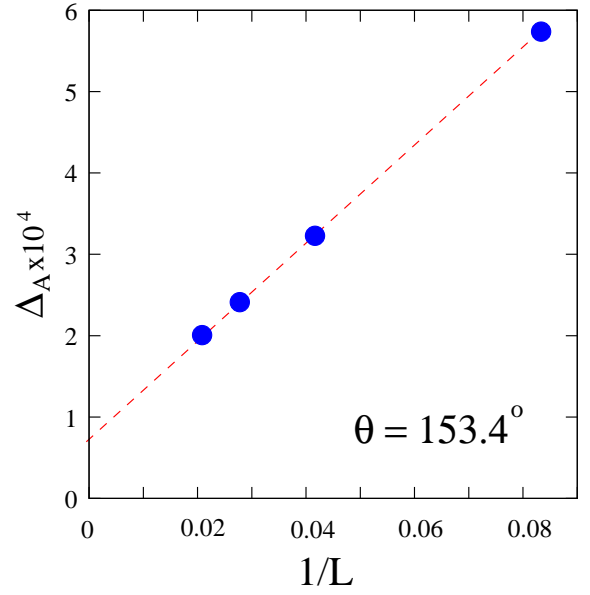


Fig. 4. (Color online) Finite-size scaling of the AFM gap $\Delta_A = E(M_0 + 1) - E(M_0)$ above the plateau state with magnetization $m_0 \equiv M_0/L = \frac{5}{3}$ (DMRG, OBC).

S_{2n} . Thus, as a first approximation, $S_{2n} + \sigma_{2n-1}$ ($n = 1, \dots, L$) can be treated as a spin-1 operator located at the n -th unit cell. Respectively, the low-energy sector of the chain can be analyzed by using the projected Hamiltonian $\mathcal{H}_{\text{eff}} = Q^\dagger \mathcal{H} Q$, where the operator Q is defined as

$$Q = \prod_{n=1}^L Q_n, \quad Q_n = \sum_{\alpha_n=0,\pm} |\alpha_n\rangle \langle \alpha_n|.$$

Here $|\alpha_n\rangle$ ($\alpha_n = 0, \pm$) are the canonical basis states of the composite-spin operator $S_{2n} + \sigma_{2n-1}$ in the spin-1 subspace. In terms of the Ising states $|S_{2n}^z, \sigma_{2n-1}^z\rangle$ the basis states $|\alpha_n\rangle$ read

$$\begin{aligned} |0\rangle_n &= \frac{1}{\sqrt{2}} \left(\left| -\frac{1}{2}, \frac{1}{2} \right\rangle - \left| \frac{1}{2}, -\frac{1}{2} \right\rangle \right) \\ |\pm\rangle_n &= \frac{1}{2} \left(\mp \sqrt{3} \left| \pm \frac{3}{2}, \mp \frac{1}{2} \right\rangle \pm \left| \pm \frac{1}{2}, \pm \frac{1}{2} \right\rangle \right), \end{aligned} \quad (2)$$

where for simplicity we have omitted the cell index n on the right-hand side of the equations.

Calculating the matrix elements of the operators S_{2n} and σ_{2n-1} in the basis (2), one obtains

$$Q_n^\dagger S_{2n} Q_n = \frac{5}{4} S'_n, \quad Q_n^\dagger \sigma_{2n-1} Q_n = -\frac{1}{4} S'_n, \quad (3)$$

where the effective spin-1 operators S' are defined as follows: $S'^z = |+\rangle\langle+| - |-\rangle\langle-|$, $S'^+ = \sqrt{2}(|+\rangle\langle 0| + |0\rangle\langle-|)$, and $S'^- = (S'^+)^\dagger$ for each unit cell. Finally, a substitution of Eqs. (3) in the expression for \mathcal{H}_{eff} leads to the following effective Hamiltonian

$$\mathcal{H}_{\text{eff}} = -\frac{5}{4} J_1 L + J_{\text{eff}} \sum_{n=1}^L S'_n \cdot S'_{n+1}, \quad (4)$$

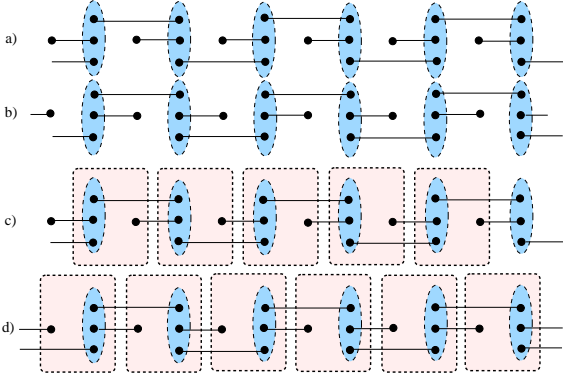


Fig. 5. (Color online) Valence-bond-solid picture of the doubly degenerate non-magnetic phases according to Eq. (5) in the limits $|J_F| \ll J_{AF}$ (a,b) and $|J_F| \gg J_{AF}$ (c,d). The small black dots denote spin- $\frac{1}{2}$ variables. The lines between two spins $\frac{1}{2}$ denote a singlet bond, whereas the dashed ellipses and rectangles denote symmetrization of the spin- $\frac{1}{2}$ variables. The first two (the last two) VBS states approximately represent ground states of the open spin-1 (spin-2) AFM Heisenberg chain. In the intermediate region ($|J_F| \approx J_{AF}$) only a part the composite cell spins form spin-2 states.

where $J_{\text{eff}} = \frac{5}{16} (\frac{5}{2} J_2 - J_1)$.

As a matter of fact, Eq. (4) coincides with the first-order effective Hamiltonian resulting from the decoupled-dimer limit defined by the Hamiltonian $\mathcal{H}_0 = J_1 \sum_{n=1}^L \mathbf{S}_{2n} \cdot \boldsymbol{\sigma}_{2n-1}$. Depending on the sign of J_{eff} , the above Hamiltonian supports a gapped Haldane-type phase ($J_{\text{eff}} > 0$) and a partially-polarized FiM phase ($J_{\text{eff}} < 0$). The transition point at $J_{\text{eff}} = 0$ (i.e., $\theta = 21.8^\circ$) corresponds to a completely dimerized GS constructed from independent spin-1 dimers. This point is related to the numerically established phase boundary at $\theta = \theta_2$.

In Figure 5(a,b) we present the suggested valence-bond-solid (VBS) states $|\Psi_L\rangle$ and $|\Psi_R\rangle$ implementing the discussed dimerization features of the GS. Under OBC, there are two such states depending on the position of the AFM bond in the three-spin clusters $\boldsymbol{\sigma}_{2n-1} - \mathbf{S}_{2n} - \boldsymbol{\sigma}_{2n+1}$ ($n = 1, \dots, L$). Using the Schwinger representation for an arbitrary spin- S operator with two types of commuting bosons (i.e., $S^+ = a^\dagger b$, $S^z = a^\dagger a - b^\dagger b$, where $a^\dagger a + b^\dagger b = 2S$), the related VBS state $|\Psi_L\rangle$ for a periodic chain can be written in the form

$$|\Psi_L\rangle = \prod_{n=1}^L (a_{2n}^\dagger b_{2n+2}^\dagger - b_{2n}^\dagger a_{2n+2}^\dagger)(a_{2n-1}^\dagger b_{2n}^\dagger - b_{2n-1}^\dagger a_{2n}^\dagger) |0\rangle.$$

Here $a_i^\dagger a_i + b_i^\dagger b_i = 2S$ (2σ) for $i = 2n$ ($i = 2n-1$) and $|0\rangle$ is the vacuum boson state. Notice that the states $|\Psi_L\rangle$ and $|\Psi_R\rangle$ for an open chain have different number of "dangling" spin- $\frac{1}{2}$ free bonds suggesting different degeneracy of the GS in the thermodynamic limit. This fact may explain the observed automatic selection of one of both states in the DMRG simulations (see, e.g., Figure 2) and considerably complicates the analysis of the low-energy sector for open chains.

The dimerization effect of the three-body interaction in the whole interval $\theta_2 < \theta < \theta_3$ can be approximately studied by a simple decoupling of the three-body terms in the original Hamiltonian (1):

$$\begin{aligned} & (\mathbf{S}_{2n} \cdot \boldsymbol{\sigma}_{2n-1})(\mathbf{S}_{2n} \cdot \boldsymbol{\sigma}_{2n+1}) + \text{h.c.} \\ &= 2C_L (\mathbf{S}_{2n} \cdot \boldsymbol{\sigma}_{2n+1}) + 2C_R (\mathbf{S}_{2n} \cdot \boldsymbol{\sigma}_{2n-1}) - 2C_L C_R. \end{aligned}$$

Substituting the above expression in Eq. (1), we obtain the following "mean-field" spin Hamiltonian with alternating FM-AFM exchange bonds

$$\mathcal{H}_{\text{MF}} = \sum_{n=1}^L [J_{AF} (\mathbf{S}_{2n} \cdot \boldsymbol{\sigma}_{2n-1}) + J_F (\mathbf{S}_{2n} \cdot \boldsymbol{\sigma}_{2n+1})] - E_0, \quad (5)$$

where $J_{AF} = J_1 + 2C_R J_2$, $J_F = J_1 + 2C_L J_2$, and $E_0 = 2L J_2 C_L C_R$. Note that the decoupling procedure violates the translational symmetry of the original Hamiltonian (1). Since the unit cell in Eq. (5) is doubled, there is a pair of such Hamiltonians (connected by the symmetry transformation $J_F \longleftrightarrow J_{AF}$) related to both types of dimerization functions ($|\Psi_{L,R}\rangle$) introduced above. The decoupling procedure can be roughly justified by noting that almost in the whole non-magnetic interval the values of C_L are close to the eigenvalue $-\frac{5}{4}$ of the operator $\mathbf{S}_{2n} \cdot \boldsymbol{\sigma}_{2n-1}$ (see Figure 2). This approximately implies spin-1 states in the unit cells for each $n = 1, \dots, L$. In the spin-1 subspace, the matrix elements of the three-body term in Eq. (1) coincide with the matrix elements of the Heisenberg term $-\frac{5}{2} J_2 \sum_{n=1}^L \mathbf{S}_{2n} \cdot \boldsymbol{\sigma}_{2n+1}$, so that the basic operator structure of Eq. (5) can be reproduced.

In approaching the phase boundary θ_2 , the coupling constant J_F goes to zero (see Figure 6), so that in this case the decoupled-dimer limit becomes a valid approximation. Up to first order in $|J_F|/J_{AF}$, the Hamiltonian \mathcal{H}_{MF} is equivalent to the projected spin-1 Hamiltonian (4) with $J_{\text{eff}} = -\frac{5}{16} J_F$ ($J_{\text{eff}} > 0$). The obtained phase boundary (now defined as $J_F = 0$) surprisingly well reproduces the numerical estimate $\theta_2 = 25.5^\circ$. As far as the parameter $|J_F|$ increases with θ , it seems relevant to evaluate the effect of the second-order perturbation in $|J_F|/J_{AF}$, as well. However, such a perturbation does not lead to any qualitative changes of the GS because its effect is restricted to a small renormalization of J_{eff} and to appearance of an irrelevant (FM) next-nearest-neighbor Heisenberg term in Eq. (5). Actually, for larger $|J_F|$ it is instructive to analyze the other decoupled-dimer limit of Eq. (5) based on non-interacting (FM) spin-2 dimers and using the small parameter $J_{AF}/|J_F| \ll 1$. Up to first order in $J_{AF}/|J_F|$, this gives Eq. (4), but now with the AFM coupling $J_{\text{eff}} = \frac{3}{16} J_{AF}$ and the effective spin-2 operators \mathbf{S}'_n . In terms of VBS states, the formation of local spin-2 states corresponds to an additional symmetrization of the cell spins, as shown in Figure 5(c,d), without any abrupt change in the topological structure of the singlet bonds. Therefore, it may be speculated that the transition between both dimer limits is realized through a smooth crossover between both Haldane-type gapped states.²

² The alternating-bond FM-AFM Heisenberg chain (5), describing a smooth transition between the spin-1 and spin-2

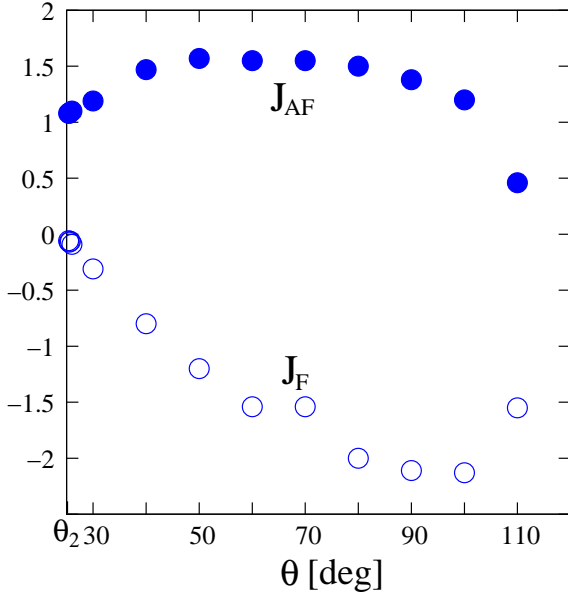


Fig. 6. (Color online) The effective exchange constants J_F and J_{AF} in the Hamiltonian \mathcal{H}_{MF} as functions of θ .

In Figure 7 we present numerical results for the triplet energy gap Δ_T in the discussed parameter region. The growth of the gap approximately up to $\theta \approx 45^\circ$ can be related with the established increase of the effective exchange constant J_{eff} in Eq. (4). In accord with the suggested VBS state in Figure 5(a), for OBC one observes the expected structure of the lowest excited states including a singlet GS, which is degenerate with the Kennedy edge triplet in the thermodynamic limit [19]. The first bulk excitation, related to the Haldane gap, appears as a spin-2 (quintet) state resulting from the combination of the bulk and Kennedy's edge triplets. On the other hand, for $\theta > 45^\circ$ the structure of the lowest excited states becomes very complicated due to the presence of many parasitic edge excitations. Namely, as demonstrated in Figure 5(b,c,d), the number of free edge spins and their values depend on (i) the type of established VBS states ($|\psi_L\rangle$ or $|\psi_R\rangle$) and (ii) the increased tendency (with θ) towards formation of local spin-2 states. For this reason, for larger θ the gap Δ_T is presented for periodic chains. Since the increase of $|J_f|$ is restricted to $|J_f| \lesssim 2$, the true spin-2 dimer limit is not reached. Nevertheless, as far as the pure spin-2 phase is characterized by an extremely small energy gap $\Delta = 0.085(5)J$ according to the DMRG result in Ref. [20]—it is reasonable to admit that the established decrease of Δ_T for $\theta \gtrsim 45^\circ$ is connected with a smooth crossover between the spin-1 and the spin-2 Haldane-type non-magnetic states. Finally, due to the extremely small gap Δ_T and the large number of low-lying energy states, it is difficult to give a precise DMRG estimate for the other phase boundary θ_3 and the properties of the GS close to this boundary.

Haldane phases, deserves a special detailed analysis going beyond the scope of the present study.

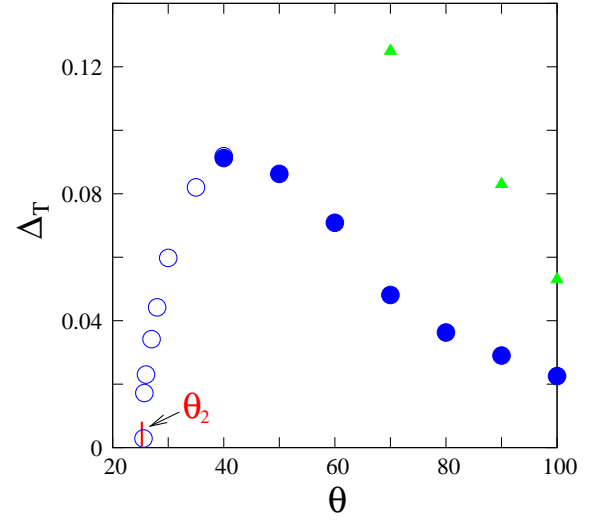


Fig. 7. (Color online) The extrapolated (up to $L = 60$) triplet gap Δ_T vs θ in the SL state calculated by DMRG under OBC (open circles) and PBC (filled circles). The filled triangles denote the quintet gap under PBC.

3 Summary

We have established the general structure of the quantum phase diagram of the alternating-spin $S = \frac{3}{2}$ and $\sigma = \frac{1}{2}$ Heisenberg chain with extra isotropic three-body exchange interactions. To some extent the established partially-polarized FiM phases resemble the magnetic phases of the extreme quantum chain with alternating spins $S = 1$ and $\sigma = \frac{1}{2}$ [15], apart from the vicinity of the FM point θ_F where both systems support different plateau states. On the other hand, due to the clustering effect of the three-body interactions, both models support completely different quantum phases in the non-magnetic region of the phase diagram: the critical phase in the $(1, \frac{1}{2})$ model is replaced by a specific doubly-degenerate phase, which can be described as a Haldane-type gapped state predominantly composed of effective cell spins with quantum spin numbers 1 or 2. It may be expected that most of the predicted effects and phases persist in higher space dimensions.

Acknowledgment

This work was supported by the Deutsche Forschungsgemeinschaft (SCHN 615/20-1) and by an exchange program between Germany and Bulgaria (DAAD PPP Bulgarien 57085392 & DNTS/Germany/01/2). S. P. was partially supported by DAAD (PPP Project ID 57067781), the FSP AMMO at the University of Applied Sciences in Bielefeld, and the Bulgarian NSF (Grant DFNI I-01/5). We thank J. Ummethum for help with the DMRG program.

References

1. F. Michaud, F. Vernay, S. R. Manmana, F. Mila, Phys. Rev. Lett. **108**, 127202 (2012)

2. *Introduction to Frustrated Magnetism: Materials, Experiments, Theory*, edited by C. Lacroix, P. Mendels, F. Mila, Springer Series in Solid-State Sciences, Vol. 164 (2011)
3. A. Furrer, Int. J. Mod. Phys. B **24**, 3653 (2010)
4. A. Furrer, O. Waldmann, Rev. Mod. Phys. **85**, 367 (2013)
5. U. Falk, A. Furrer, J. K. Kjems, H. U. Güdel, Phys. Rev. Lett. **52**, 1336 (1984)
6. F. Michaud, S. R. Manmana, F. Mila, Phys. Rev. B **87**, 140404(R) (2013)
7. N. B. Ivanov, J. Ummethum, J. Schnack, Eur. Phys. J. B **87**, 226 (2014)
8. N. B. Ivanov, J. Schnack, J. Phys.: Conf. Series **558**, 012015 (2014)
9. F. Michaud, F. Mila, Phys. Rev. B **88**, 094435 (2013)
10. S. R. White, Phys. Rev. Lett. **69**, 2863 (1992)
11. J. Ummethum, *Calculation of static and dynamical properties of giant magnetic molecules using DMRG*, Ph.D. thesis, Bielefeld University (2012)
12. J. Ummethum, J. Nehrkorn, S. Mukherjee, N. B. Ivanov, S. Stuißer, Th. Strässle, P. L. W. Tregenna-Piggott, H. Mutka, G. Christou, O. Waldmann, J. Schnack, Phys. Rev. B **86**, 104403 (2012)
13. Z.-Y. Wang, S. C. Furuya, M. Nakamura, R. Komakura, Phys. Rev. B **88**, 224419 (2013)
14. R. Thomale, S. Rachel, P. Schmitteckert, M. Greiter, Phys. Rev. B **85**, 195149 (2012)
15. N. B. Ivanov, J. Richter, Phys. Rev. B **69**, 214420 (2004)
16. see, e.g., T. Shimokawa, H. Nakano, J. Kor. Phys. Soc. (SI) **63**, 591 (2013) and references therein
17. Sh.S. Furuya, Th. Giamarchi, Phys. Rev. B **89**, 205131 (2014)
18. M. Oshikawa, M. Yamanaka, I. Affleck, Phys. Rev. Lett. **78**, 1984 (1997)
19. T. Kennedy, J. Phys. Condens. Matter **2**, 5737 (1990)
20. U. Schollwöck, O. Golinelli, Th. Jolicoeur, Phys. Rev. B **54**, 4038 (1996)